Available online at www.sciencedirect.com

ScienceDirect

journal homepage: www.elsevier.com/locate/he

Propulsion of a hydrogen-fuelled LH_2 tanker ship

Abdullah NFNR. Alkhaledi [a,b,*], *Suresh Sampath* [a], *Pericles Pilidis* [a]

[a] *Thermal Power & Propulsion Engineering, Cranfield University, Bedfordshire, MK430AL, United Kingdom*
[b] *Department of Automotive and Marine Engineering, College of Technological Studies, PAAET, P.O. Box 42325 Shuwaikh, Kuwait*

HIGHLIGHTS

- H_2 fuelled propulsion can be considered as a solution for a marine zero-emission target.
- TurboMatch analytical method achieved H_2 fuelled propulsion system evaluation.
- Azimuthal thruster is suitable for a large-scale liquid-hydrogen tanker ship design.
- COGAS can ensure LH2 tanker ships power requirements at variant conditions.
- Technical feasibility Hydrogen-fuelled propulsion system can be applicable for the future.

GRAPHICAL ABSTRACT

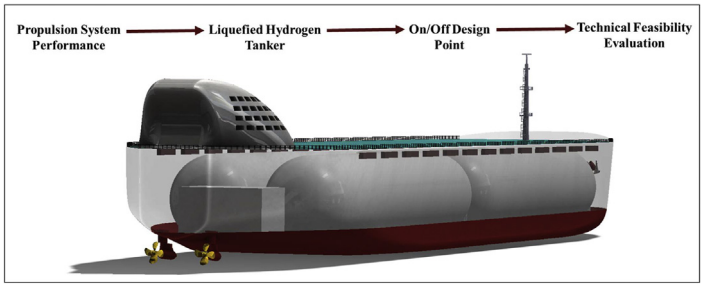

ARTICLE INFO

Article history:
Received 19 September 2021
Received in revised form
15 February 2022
Accepted 22 March 2022
Available online 12 April 2022

Keywords:
Liquefied hydrogen
LH_2 tanker
Ship design
Liquid hydrogen tank
Propulsion system

ABSTRACT

This study aims to present a philosophical and quantitative perspective of a propulsion system for a large-scale hydrogen-fuelled liquid-hydrogen (LH2) tanker ship. Established methods are used to evaluate the design and performance of an LH2-carrier propulsion system for JAMILA, a ship designed with four cylindrical LH2 tanks bearing a total capacity of ~280,000 m^3 along with cargo and using the boil-off as propulsion and power fuel. Additionally, the ship propulsion system is evaluated based on the ship resistance requirements, and a hydrogen-fuelled combined-cycle gas turbine is modelled to achieve the dual objectives of high efficiency and zero-carbon footprint. The required inputs primarily involve the off-design and degraded performance of the gas-turbine topping cycle, and the proposed power plant operates with a total output power of 50 M.W. The results reveal that the output power allows ship operation at a great speed even with a degraded engine and adverse ambient conditions.

* *Corresponding author*. Thermal Power & Propulsion Engineering, Cranfield University, Bedfordshire, MK430AL, United Kingdom.
E-mail address: alkaaledi@gmail.com (A.NFNR. Alkhaledi).

https://doi.org/10.1016/j.ijhydene.2022.03.224

Nomenclature

Symbol:	*Meaning*
A_{BT}	Transverse bulb area
A_E/A_O	Propeller blade area ratio
A_T	Immersed part of the transverse sectional area of transom at A.P. at zero speed
B	Ship breadth extreme
C	Coefficient that accounts for the specific shape of the afterbody
C_A	Correlation allowance coefficient
C_B	Block coefficient
C_F	Frictional resistance coefficient
C_m	Midship section area coefficient
C_p	Prismatic coefficient
c_p	Specific heat constant pressure
c_{stern}	After body coefficient
C_{Wp}	Waterplane area coefficient
D	Ship depth
D.P	Design point
D_{pr}	propeller diameter and
DWT	Ship deadweight
F_n	Froude number
g	Gravitational acceleration
GTCC/COGAS	Gas turbine combined cycle
h	Value of shaft immersion depth
h_a	Superheat steam enthalpy
h_B	Vertical position of the centroid of A_{BT} above the baseline
h_d	Economiser outlet enthalpy
h_i	Steam turbine input enthalpy
h_{oiso}	Isentropic outlet steam enthalpy
h_{oact}	Actual outlet steam enthalpy
h_{of}	Fluid outlet steam enthalpy
h_{ofg}	Fluid and gas outlet steam enthalpy
i_E	Angle of the waterline at the bow
J	Advance ratio
K_Q	Propeller torque coefficients
K_T	Propeller thrust coefficients
LBP	Length between perpendicular
lcb	Longitudinal centre of bouncy
LH2	Liquefied hydrogen
LNG	Liquefied natural gas
LOA	Length overall
$L_{.R.}$	Length of the run
L.W.	Length of water line
LWT	Ship lightweight
m_g	Gas mass flowrate
m_s	Steam mass flowrate
NOx	Nitrogen oxide
n	Revolutions of propeller per second
OD. 1	Off design point
P/D_{pr}	Propeller pitch to diameter ratio
P_{atm}	Atmospheric pressure
P_{BH}	Brake horsepower
P_{cond}	Condenser pressure
P_{DH}	Propulsive horsepower
P_{EH}	Effective horsepower
P_S	Steam pressure
P_{TH}	Ship required thrust horsepower
P_v	Vapor pressure of water

Symbol	*Meaning*
Q	Propeller torque
$Q_{3-4} = Q_{e-d}$	Heat transfer in gas side from heat recovery steam generator (HRSG)
Q_{1-3}	Heat exchanged above the pinch
R_A	Model-ship correlation resistance
R_{APP}	Appendage resistance
R_B	Additional pressure resistance of bulbous bow
R_F	Frictional resistance
$R_F(1+k_1)$	Viscous hull resistance
R_n	Reynolds number
R_T	Total resistance
R_{TR}	Additional pressure resistance of the immersed transom stern
R_W	Wave resistance
S_{APP}	Wetted surface area of appendage
S_{BH}	Wetted surface area of bare hull
S_i	Steam turbine input entropy
S_o	Steam turbine outlet entropy
S_{og}	Gas outlet steam entropy
S_{of}	Fluid outlet steam entropy
T	Ship draft
t	Thrust dedication factor
t/c	Thickness to chord length ratio
T_a	Superheat temperature
T_c	T_b Saturation temperatures
T_d	Economiser outlet temperature
T_e	Feed water temperature
T_F	Forward draught of the ship
T_H	Propeller thrust required
T_{Hg}	Propeller thrust generated
T_1	Gas turbine exhaust temperature
T_3	Pinch point temperature on gas side
T_4	Stack temperature
V	Ship speed
υ	seawater kinematic viscosity
V_A	speed of advance
w	Effective wake fraction
W_{CC}	Total combined cycle output power
W_{GT}	Gas turbine output power
W_{pump}	Pump work
W_{ST}	Steam turbine output power
X	Outlet steam quality
Z	Propeller blade number
ΔT_a	Approach point temperature difference
ΔT_p	Pinch point temperature difference
Δ_{total}	Ship total displacement
∇	Displacement volume of the ship
η_{CC}	Total combined cycle output efficiency
η_H	Hull efficiency
η_R	Relative rotative efficiency
η_{ST}	Steam turbine isentropic efficiency
η_T	Transmission efficiency
η_o	Propeller efficiency in open water

λ	Wavelength of the dynamic load case	$1+k_1$	Form factor
ρ	The density of the sea water	$1+k_2$	Appendage resistance factor

Introduction

The International Maritime Organization (IMO)—the U.N. agency responsible for the safety of lives at sea, efficient shipping, and the prevention of pollution produced from international shipping—has drafted strict environmental regulations to reduce the impact of maritime shipping emissions on the global environment. In April 2018, the IMO adopted an initial strategy to reduce greenhouse gas (GHG) emissions from international maritime shipping by at least 50% by 2050 as compared to 2008 levels. This strategy additionally targets reducing CO_2 emissions from shipping by at least 40% and 70% by 2030 and 2050, respectively, as compared to 2008 levels [1]. This will reduce CO_2 emissions by maritime shipping, thereby decreasing its impact on the environment. Therefore, certain countries have already begun applying these new IMO regulations. Based on these new regulations, the United Kingdom published the U.K. Clean Maritime Plan in July 2019 to serve as an environmental road map and achieve the government's Maritime 2050 vision that intended to transition shipping in the U.K. waters to a zero-emissions future, wherein all new vessels in U.K. waters will be designed with zero-emissions propulsion capabilities by 2025 [2]. Accordingly, the development of alternative fuels and technologies is imminent to reduce maritime shipping emissions and address new international- and national-level requirements. In this context, liquefied hydrogen (LH2) is gaining popularity as a considerable option for achieving the zero-carbon target of marine applications to ensure decarbonisation of the maritime sector in the future [3].

Hydrogen fuel can be potentially used for decarbonising thermal engines, provided the production of hydrogen is a carbon-free process and the engines deliver very low amounts of NOx. In addition, hydrogen removes additional harmful emissions such as unburnt hydrocarbons, aromatic compounds, sulphur oxides, soot, and smoke. Hydrogen is a technology solution to provide sustainability in the maritime environment. However, unlike fossil fuels, hydrogen gas cannot be directly extracted from the earth but must be manufactured from various sources. In general, hydrogen can be produced from several sources, including water, biomass, and fossil fuels, using electrolysis, steam–methane reforming, and gasification [4,5]. However, technologies that can produce hydrogen in cleaner ways are emerging. For instance, an electrolysis process that is a zero-CO_2 emissions technology has been developed to produce hydrogen by splitting water into hydrogen and oxygen directly without natural gas or CO_2 emissions by using solar energy [6]. Currently, global efforts are intending to produce a low-emission propulsion system as well as include carrying clean energy through hydrogen using large tanker ships [3]. In the future, hydrogen will be transported using a large-scale LH2 carrier ship. However, saving weight and cargo space is a concerning issue in the maritime sector, especially for LH2 tankers, because the density of hydrogen is extremely less as a voluminous substance. Thus, a combined-cycle gas turbine is a potential alternative for achieving compact engine size benefits with acceptable thermal efficiency targets [7].

Prior related research focuses on designing and evaluating a combined-cycle gas turbine as a marine propulsion system. In 2000, the 'Millennium' cruise ship was launched, which operates on a combined cycle including two 25-MW "LM2500+" gas turbines fuelled by marine gas oil (MGO) and a 9-MW steam turbine as a bottoming cycle [8,9]. In addition, Benvenuto et al. [10] developed mathematical models to optimise and compare the performance of several possible steam cycle configurations to employ a COGAS power plant for marine propulsion. The overall energy conversion efficiency of the installation, plant dimensions, weights, and economic considerations were all accounted as critical parameters in selecting a propulsion system.

However, Benvenuto et al. study provide vital fundamental information for evaluating the performance of marine COGAS propulsion systems without using liquefied hydrogen fuel [10,11]. The following research and projects aim at hydrogen as a ship propulsion system fuel to achieve emission reduction sustainability to protect the global from climate change expansion. Evrin and Dincer [36] integrated a hydrogen-fuelled fuel cell with a steam producing cycle to supply ships electricity and freshwater using two heat recovery systems to provide ship thrust and drive the ship refrigeration cycle and assessed that the proposed model system vastly reduces greenhouse-gas emission. Feng Li et al. [37] Applied a numerical calculation using Fluent software to simulate the leakage and diffusion of hydrogen in a fuel cell ship and analyse the concentration distributions of hydrogen in the ship cabins under various ventilation circumstances to offer a guide for the design of a fuel cell ship utilising high-pressure gaseous hydrogen. Mao X et al. [38] targeted a passenger ship powered by a hydrogen fuel cell and applied a numerical simulation on the leakage and explosion of hydrogen in different compartments on a ship using fluid computation software. McKinlay et al. [39] analysed the applicability of hydrogen fuel cells to be a suitable method of decarbonising the auxiliary services of current long-distance ships using LNG tanker data. This research has indicated that retrofitting a hydrogen fuel cell system to a current large-scale ship might theoretically make a meaningful reduction of emissions by meeting auxiliary load. In another study, McKinlay et al. [40] evaluated various viable options to achieve ships zero-emission propulsion target by 2025, with three promising alternative fuels hydrogens, ammonia and methanol. This is essentially owing to their possibility to generate emission-free electricity by using fuel cells. To the best of the authors' knowledge, the design and performance evaluation of hydrogen-fuelled combined-cycle gas turbines for marine

applications has not been considered yet. Thus, the preliminary design of the hydrogen carrier ship [3] is required to be completed based on the prime-mover system of the LH2 tanker ship, including the performance evaluation of a hydrogen-fuelled combined-cycle gas turbine as a maritime propulsion system.

This study aims to design and evaluate the performance of a hydrogen-tanker ship-propulsion system in design and off-design conditions. Using state-of-the-art design and analysis methods, the authors delivered on the prospect of such a ship propulsion system. However, the economic and cost analysis for the LH2 propulsion system was beyond the scope of the current study. The feasibility aspect of the propulsion system was analysed using the Techno-economic Environmental Risk Analysis (TERA) method [12,13] and will be the focus of another manuscript in the future.

Design and performance differences with a conventional combined-cycle gas turbine

This research proposes an extraordinary, philosophical approach to achieve zero-emission maritime transportation through design and performance assessment of untraditional combined cycle gas turbine as an LH2 tanker prime mover. Thus, the approach suggested in this research is a derivative design, not a retrofit. Technically, the design and performance of the combined cycle gas turbine were evaluated using TURBOMATCH (inhouse Cranfield gas turbine performance simulation code) [18] by applying conventional and hydrogen fuels. The TURBOMATCH analytical method utilises the performance principles of a gas turbine [41] and is a reiterative method based on gas turbine components characteristics. As estimated, there are no main variations caused by utilising hydrogen fuel in the engine performance compared with conventional fuel, as shown in Table 1.

Engine performance assessment

In order to characterise the difference of design method for hydrogen-fuelled combined-cycle gas turbine and conventional combined-cycle gas turbine, the authors selected the design point (D.P) of the COGAS fuelled by hydrogen as a ship prime mover based on engine simulation and the results of performance analysis in terms of gas turbine efficiency, specific power, and COGAS efficiency through the compressor pressure ratio variation at constant turbine entry temperature value (1550 K) in case of using hydrogen fuel and conventional fuel which is shown in Fig. 1. The results were indicated that the COGAS fuelled by hydrogen could achieve 55% as the highest efficiency with the compressor pressure ratio of 23.1 for the gas turbine design point. Moreover, Fig. 1 shows that using hydrogen fuel achieved 4.5% higher specific work than conventional fuel due to combustion products containing no CO_2 and a larger quantity of H_2O, which has a higher specific heat at constant pressure value [42].

Table 1 – Gas turbine engine characteristics by applying conventional and hydrogen fuel.

Gas turbine characteristics	Conventional	Hydrogen	Units
Fuel flow	1.852	0.7485	kg/s
Mass flow	84.2	84.2	kg/s
Turbine entry temperature	1550	1550	K
Output power	34.7	36.2	MW
Exhaust mass flow	85.9	84.9	kg/s
Exhaust gas temperature	845.06	840.3	K
Compressor pressure ratio	23.1	23.1	–
COGAS			
Output power	48	50	MW
Thermal efficiency	54.5	55	%

Hydrogen gas turbine design

The gas turbine engine design fuelled by hydrogen was inspired by an LM2500+ industrial gas turbine engine fuelled by natural gas [28] as conventional fuel to achieve the ships power requirement. The design difference arises during the slightly different properties in the hot section of the gas turbine fuelled by hydrogen due to the same reason related to the combustion products containing no CO_2. Table 2 shows the changes in the gas turbine hot section areas with the velocity variation for each stage. The gas turbine fuelled by hydrogen simulation results shows that the combustor outlet and turbine inlet section's area increased around 3.1% compared with conventional fuel in the combustor. On the other hand, in the case of turbine outlet and power turbine inlet using hydrogen fuel, the section's area decreased around 0.002 m^2 compared with conventional fuel. In the case of a power turbine outlet using hydrogen fuel, the section's area increased around 1.6% compared with conventional fuel. Those changes are due to variability in each section's total inlet and outlet temperatures.

Overall design philosophy description

Based on the preliminary design of the LH2 tanker ship hull and the stability analysis conducted in a previous study [3], a suitable propulsion system design is required for this unique ship. The authors of this paper determined that the initial design concept of the LH2-tanker ship-propulsion system depends on several factors based on the ship propulsion power requirements, such as ship dimensions, weights, resistance, speed, and hull design coefficients, considering the decarbonisation target and high thermal efficiency achievement. The primary stage of the ship propulsion system design includes the ship-module calculation of the brake power required from the propulsion system, prediction of ship hull resistance, and estimation of propulsion factors using a statistical method [14,15]. In particular, the total hull resistance was preliminarily calculated as a function of viscous hull resistance, appendage resistance, wave resistance, and model-ship correlation resistance, including the additional pressure resistance of bulbous bow near the water surface, which was assumed as zero owing to the ship hull form design. Moreover, the additional pressure resistance of the immersed transom stern was assumed as zero owing to the ship design. The calculation of propulsion factors involved the

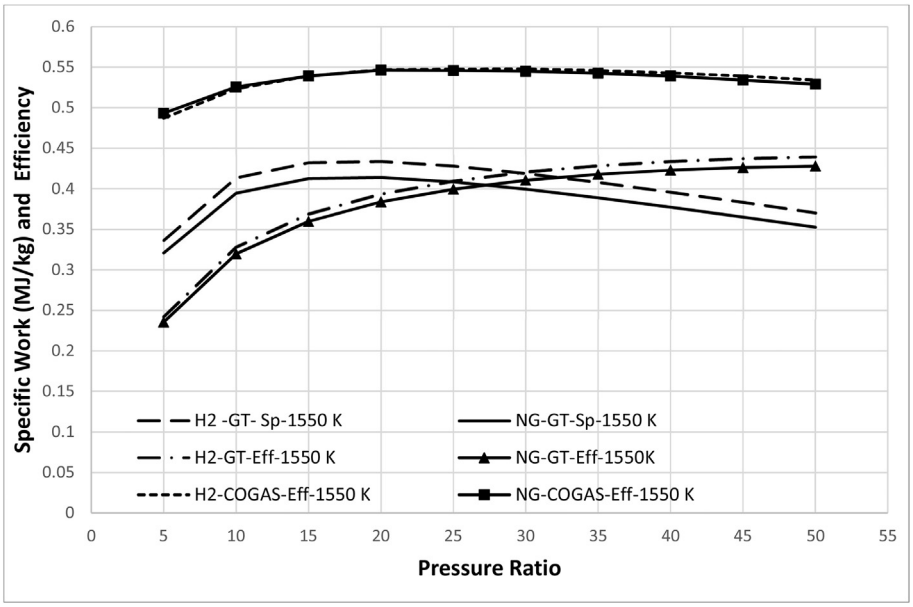

Fig. 1 – The specific work for gas turbine and efficiencies for the gas turbine and COGAS for various pressure ratios using conventional and hydrogen fuel in design point.

Table 2 – Gas turbine hot section area changes in different velocities using conventional and hydrogen fuel.

Station	Velocity (m/s)	Conventional (m^2)	Hydrogen (m^2)
Combustor outlet	304	0.062	0.064
Turbine inlet	304	0.062	0.064
Turbine outlet	265	0.216	0.214
Power turbine inlet	265	0.216	0.214
Power turbine outlet	224	0.925	0.940

prediction of the effective wake fraction, thrust deduction factor, and the relative rotational efficiency of the propulsion system established on the LH2 carrier ship. In addition, the resistance estimation and the power required during loading and unloading conditions at various speeds were validated using the MAXSURF software.

Furthermore, the collaboration between the hull and propeller was represented via the power required by the combined-cycle gas turbine—known as the brake power from the effective power for the ship hull, which is a product of the total resistance and the LH2 carrier ship speed. The authors used the Wageningen B-series propellers method to estimate the twin-screw attached to the pods of the open-water propeller design and specify its characteristics [16]. However, the lightweight of hydrogen requires a distinct ship design, especially a small hull draft in the unloading condition, which eventually causes operation challenges in shallow water as compared to alternative tanker ships. Based on this distinct condition, the authors of this paper selected a turboelectric system including two azimuthal podded propellers with a maximum power output of 15.5 MW each as a component of the LH2 carrier ship propulsion system. This selection supported the reliability and controllability of the LH2 carrier ship in shallow waters. After the power requirements were determined, the power plant was required to be modelled for generating the power required for the vessel. Thus, the authors selected a hydrogen-fuelled combined-cycle gas turbine as the prime mover to generate power for the LH2 propulsion system owing to its more compact size and dimensions, which is a vital consideration for the large volume of LH2 cargo, lightweight, high thermal efficiency, and low emissions in comparison to two-stroke diesel engines [17]. The combined-cycle gas turbine, including a simple-cycle gas turbine and a single-pressure heat-recovery steam generator, was simulated with the capabilities of design and off-design point calculations based on the TURBOMATCH gas-turbine performance code [18] and MATLAB software. The following sections will describe the power requirements, power generated, and engine efficiency for LH2 carrier ships in various conditions. The results of the preliminary design evaluation are listed in Table 3 [3].

Power requirements

As listed in Table 3, the estimation of the primary ship parameters [3] was followed by the investigation to establish the power plant requirements. From the outset, the authors decided to use a combined-cycle gas turbine as the prime mover for the LH2 tanker ship to achieve high thermal efficiency with low NOx signatures from the hydrogen gas turbines to satisfy the significant investments and efforts towards NOx abatement [19]. Therefore, the authors selected a large-scale LH2 carrier ship with a capacity of 280,000 m^3 for suitability towards the global future energy demand [3]. Moreover, the hydrogen volume (280,000 m^3) was divided into four tanks—each of 70,000 m^3 capacity—with a total weight of 107,000 tons for all tanks, including cargo that assists the ship

Table 3 – Ship parameters and power input data.

LH2 tanker parameter	Value	Unit
Class	JAMILA	–
Vessel type	LH_2 Tanker	–
Total displacement (Δ_{total})	232,000	tonnes
Lightweight (LWT)	210,000	tonnes
Deadweight (DWT)	22,000	tonnes
Length overall (LOA)	370	m
Length between perpendicular (LBP)	367.5	m
Length on water line (L.W.)	367.9	m
Breadth Extreme (B)	75	m
Depth (D)	35	m
Draft (T) (full load condition)	10.012	m
Draft (T) (unload condition)	9.263	m
Block coefficient ($C_{.B.}$) (full load condition)	0.819	–
Block coefficient ($C_{.B.}$) (unload condition)	0.813	–
Ship speed (V)	18	knots
Midship Section area coefficient (C_m) (full load condition)	0.995	–
Midship Section area coefficient (C_m) (unload condition)	0.994	–
Waterplane area coefficient (C_{wp}) (full load condition)	0.900	–
Waterplane area coefficient (C_{wp}) (unload condition)	0.894	–
Prismatic coefficient (C_p) (full load condition)	0.824	–
Prismatic coefficient (C_p) (unload condition)	0.818	–
Displacement volume of the ship (∇)	226341.4634	m^3
LH2 cargo tank weight (Aluminium)	87,819 (21,955 × 4)	tonnes
LH2 cargo tank capacity	282,400 (70,600 × 4)	m^3
LH2 cargo weight	20,000 (5000 × 4)	tonnes
LH2 engine fuel tank weight (Aluminium)	4370	tonnes
LH2 engine fuel tank capacity	14,099	m^3
LH2 engine fuel weight (20 day return journey + 2-day ship idle period + 100 tonne reserve)	1277.6	tonnes
Boil off rate from the cargo	0.1 (20 tonne/day)	% per day
Fuel-saving percentage due to boiling off	29%	%
Voyage range	450 to 4400	Naut mile
Minimum Propulsion Power Required	27.3	MW
Combined cycle gas & steam installed	50	M.W.

to maintain balance during the voyage. The speed of the LH2 tanker was selected as 18 knots based on two primary reasons: the boil-off from the cargo rate, which was 0.1% per day during the voyage, and the maximum speed that can be achieved using the designed combined-cycle gas turbine with generated power in design point conditions. Furthermore, increasing the shipping speed will reduce the boil-off losses and increase the ship's fuel consumption; however, there is a maximum speed limit of 18 knots according to the engine design.

Resistance prediction

In this section, the power required to achieve the service speed of 18 knots was estimated as the maximum design point speed. The calculations were initiated with a prediction of the total resistance of the JAMILA based on the shape and dimensions of the ship. In addition, the resistance and power of JAMILA were predicted using the Holtrop and Mennen method [14,15]. The total resistance can be estimated using the following equation [20].

$$R_T = R_F(1+k_1) + R_{APP} + R_W + R_A + R_B \tag{1}$$

where $R_F(1+k_1)$ represents the viscous hull resistance, R_{APP} denotes the appendage resistance, R_W denotes the wave resistance, R_A indicates the model–ship correlation resistance, and R_B represents the additional pressure resistance of the bulbous bow near the water surface, which was assumed as zero owing to the ship design. Moreover, R_{TR} denote additional pressure resistance of the immersed transom stern, which was assumed to be zero due to the ship design.

Frictional resistance (R_F)

The Reynolds number corresponding to the length of 368 m at the water line for the JAMILA is required to be evaluated.

$$R_n = \frac{V.L_W}{\upsilon} \tag{2}$$

where 1 knot is 0.5144 m/s, and the seawater kinematic viscosity (υ), according to the table in Ref. [21], was 1.1386×10^{-6} m^2/s for 15.0 C. The frictional resistance coefficient (C_F) can be calculated using the following equation.

$$C_F = \frac{0.075}{(logR_n - 2)^2} \tag{3}$$

The wetted surface area of the bare hull (S_{BH}) can be calculated with the following equation, where the transverse bulb area for JAMILA (A_{BT}) was 0 m owing to the design of the ship without a bulbous bow.

$$S_{BH} = L_W(2T+B)\sqrt{C_m}\left(0.4530 + 0.4425C_b - 0.2862C_m - \frac{0.003467B}{T} + 0.3696C_{WP}\right) + \frac{2.38A_{BT}}{C_b} \tag{4}$$

The frictional resistance can be calculated based on the following equation [22].

$$R_F = \frac{1}{2}\cdot\rho\cdot C_F\cdot S_{BH}\cdot V^2 \tag{5}$$

The following equation expresses the coefficient c accounting for the specific shape of the after-body. Although the JAMILA has a transom section stern shape, a normal stern shape was used for applying the correlations by Holtrop and Mennen [15]. As expected, the results did not cause large deviations. Thus, the form of the after-body coefficient (c_{stern}) was considered as 0.

$$c = 1 + (0.011 \cdot c_{stern}) \tag{6}$$

and the length of the run (L_R) can be calculated using the following equation.

$$\frac{L_R}{L_W} = 1 - C_p + 0.06C_p \cdot \frac{lcb}{(4C_p - 1)} \tag{7}$$

where *lcb* denotes the longitudinal position of the centre of buoyancy forward of 0.5 L_W as a percentage (%) of L_W (+) for forward and (−) for afterwards. In this study *lcb* was 3.716. The form factor $(1 + k_1)$ can be calculated using the following equation.

$$1 + k_1 = 0.93 + 0.487118c\left(\frac{B}{L_W}\right)^{1.06806}\left(\frac{T}{L_W}\right)^{0.46106}\left(\frac{L_W}{L_R}\right)^{0.121563}\left(\frac{L_W{}^3}{\nabla}\right)^{0.36486}(1 - C_p)^{-0.60247} \tag{8}$$

Appendage resistance (R_{APP})

The appendage resistance was evaluated based on the wetted surface area of appendage (S_{APP}), appendage resistance factor $(1 + k_2)$, and frictional resistance coefficient (C_F), wherein the following equation was used to approximate the values of $(1+k_2)$ as 2.8 and (S_{APP}) as 300 m^2 [15] that represent the azimuthal propulsors surface area.

$$R_{APP} = \frac{1}{2}\rho C_F S_{APP} V^2 (1 + k_2) \tag{9}$$

Wave resistance (R_w)

The Froude number of JAMILA can be calculated using the following equation:

$$F_n = \frac{V}{\sqrt{g.L_W}} \tag{10}$$

where F_n was less than 0.4, and thus, the design was in the low-speed ship range. As the value of $\left(\frac{B}{L_W}\right)$ was 0.211, the value of C_7 was equal to that of $\left(\frac{B}{L_W}\right)$. The angle of the waterline at the bow (i_E) can be obtained using the following equation.

$$i_E = 01 + 89e^{\left[-\left(\frac{L_W}{B}\right)^{0.80856}\cdot\left(1-C_{Wp}\right)^{0.30484}\cdot\left(1-C_p-0.0225lcb\right)^{0.6367}\cdot\left(\frac{L_R}{B}\right)^{0.34574}\cdot\left(\frac{100\nabla}{L_W{}^3}\right)^{0.16302}\right]} \tag{11}$$

In addition, the value of C_1 can be calculated using the following equation, where $C_7 = \left(\frac{B}{L_W}\right)$ and

$$C_1 = 2223105 \cdot C_7^{3.78613} \cdot \left(\frac{T}{B}\right)^{1.07961} \cdot (90 - i_E)^{-1.37565} \tag{12}$$

The value of the coefficient that determined the influence of the bulbous bow on the wave resistance (C_3) can be calculated using the following equation.

$$C_3 = 0.56\frac{A_{BT}^{1.5}}{\left[B \cdot T\left(0.31\sqrt{A_{BT}} + T_F - h_B\right)\right]} \tag{13}$$

The value of the coefficient accounting for the reduction wave resistance caused by the action of a bulbous bow (C_2) can be calculated using the following equation. In the present case, the coefficient (C_2) equals one owing to the absence of a bulbous bow. Therefore, the value of the bulb area (A_{BT}) was zero. This value was used to calculate the coefficient that determined the influence of the bulbous bow on the wave resistance (C_3) (see Eq. (13)), which was derived in the following equation.

$$C_2 = e^{-1.89\sqrt{C_3}} \tag{14}$$

The value of the coefficient expressed the influence of a transom stern on the wave resistance (C_5) that can be calculated using the following equation, where A_T denotes the immersed part of the transverse sectional area of transom after perpendicular (A.P.) at zero speed as 700 m^2.

$$C_5 = 1 - \frac{0.8A_T}{B \cdot T \cdot C_m} \tag{15}$$

As the value of C_p was greater than 0.8, the value of C_{16} was determined as

$$C_{16} = 1.73014 - 0.7067C_p. \tag{16}$$

For the low-speed range, m_1 can be calculated as

$$m_1 = \frac{0.0140407L_W}{T} - \frac{1.75254\nabla^{\frac{1}{3}}}{L_W} - \frac{4.79323B}{L_W} - C_{16} \tag{17}$$

where $\left(\frac{L_W{}^3}{\nabla}\right) = 239.78$ and is less than 512; $C_{15} = -1.69385$. Moreover, the value of m_4 can be calculated using the following equation.

$$m_4 = C_{15}0.4e^{-0.034F_n^{-3.29}} \tag{18}$$

As the value of $\frac{L_W}{B} = 4.9$, it is less than 12. Furthermore, the value of λ can be determined based on the following equation.

$$\lambda = 1.446C_p - \frac{0.03L_W}{B} \tag{19}$$

Now the wave resistance can be calculated using the following equation, where (d) denotes a constant value of −0.9.

$$R_w = \rho \cdot g \cdot \nabla \cdot C_1 \cdot C_2 \cdot C_5 \cdot \exp\left[m_1 \cdot F_n^d + m_4 \cdot \cos\left(\lambda F_n^{-2}\right)\right] \tag{20}$$

Model–ship correlation resistance

The value of $(T_F/L_W) = 0.025$ (<0.04), where T_F is the fore draft assumed the same as the designed (T) draft. The value of $C_4 = 0.025$. The coefficient (C_A) can be calculated using the following equation.

$$C_A = 0.006(L_W + 100)^{-0.16} - 0.00205 + 0.003\sqrt{\frac{L_W}{7.5}}C_B{}^4C_2(0.04 - C_4) \tag{21}$$

The following equation can be used to calculate the model–ship correlation resistance.

$$R_A = 1/2 \cdot C_A \cdot \rho \cdot S_{BH} \cdot V^2 \tag{22}$$

Total resistance

The total resistance of JAMILA can be calculated as follows, and the output results of the resistance calculation will be presented in Table 4

$$R_T = R_F(1+k_1) + R_{APP} + R_W + R_A \quad (23)$$

Prediction of propulsion factors

The following method [15] was used to estimate the effective wake fraction (w), thrust dedication factor (t), and the relative rotational efficiency (η_R) of the twin-screw propulsion system designed for JAMILA, where D_{pr} denotes the propeller diameter and P/D_{pr} is the propeller pitch to diameter ratio estimated based on to the shallow draft and the propeller accommodation area as 6.4 m and 1.0, respectively. In this section, the C_B, C_p, and T were considered for the unloaded ship condition.

$$w = 0.3095C_B + 10[C_F(1+k) + C_A]C_B - 0.23D_{pr}/\sqrt{BT} \quad (24)$$

$$t = 0.325C_B - 0.1885D/\sqrt{BT} \quad (25)$$

$$\eta_R = 0.9737 + 0.111(C_p - 0.0225.lcb) - 0.06325(P/D_{pr}) \quad (26)$$

Power prediction

The interactions between the hull and propeller for JAMILA can be calculated using an established method [23] as follows:

$$P_{EH} = R_T \cdot V, \quad (27)$$

where P_{EH} denotes the effective horsepower for the ship hull. The open-water test of the propeller without a hull in front of it will produce a thrust T_H at a speed of advance V_A with an open-water propeller efficiency (η_o), which can be calculated as the required thrust horsepower (P_{TH}) based on the following equations.

$$V_A = V(1-w) \quad (28)$$

$$T_H = R_T/(1-t) \quad (29)$$

$$P_{TH} = T \cdot V_A \quad (30)$$

The hull efficiency (η_H) and the propulsive horsepower (P_{DH}) can be calculated using the following equation, where η_o denotes the propeller efficiency in open water, as presented in Tables 5 and 6, respectively.

$$\eta_H = (1-w)/(1-t) \quad (31)$$

$$P_{DH} = P_{EH}/(\eta_H \cdot \eta_O \cdot \eta_R) \quad (32)$$

Finally, the brake horsepower (P_{BH}) can be calculated using the following equation, where η_T is the transmission efficiency of the propulsion and was assumed as 0.99 [20].

$$P_{BH} = \frac{P_{DH}}{\eta_T} \quad (33)$$

Fig. 2 displays the output of the ship resistance and power calculations and their variation with the ship speed. Fig. 2a–c depict the ship resistance, effective power, and power delivered to the propellers. Fig. 2d portrays the brake power or the power delivered by the propulsion engines. For a ship speed of 18 knots in completely loaded condition, a delivered power of 48.5 MW is required to enable the sailing speed of 18 knots. In the worst-case scenario, labelled as OD1, a power of 30 MW. is available in a high degradation case combined with a high ambient temperature. In this case, the ship speed will be reduced to 16 knots. The details of D.P. and OD1 are described with the power plant analysis in COGAS powerplant.

Table 4 – Output results of the resistance calculation model for the LH2 tanker design.

Resistance calculation model parameters	Value	Units
Reynolds number (R_n)	3×10^9	–
Frictional resistance coefficient (C_F)	1.33×10^{-3}	–
Wetted surface area of the bare hull (S_{BH})	28500	m^2
Frictional resistance (R_F)	1671	KN
The specific shape of the afterbody coefficient (c)	1	–
The length of the run (L_R)	96.5 m	m
Form factor ($1+k_1$)	1.32	–
Appendage resistance (R_{APP})	49.2	kN
Froude number (F_n)	0.1541	–
The angle of the waterline at the bow (i_E)	60.98	Degree
Coefficients values ($C_1, C_2, C_3, , C_5, C_{16}$)	5.1,1,0,0.19,0.15	–
The values of m_1, m_4	-1.85 , -7.77×10^{-8}	–
Wavelength of the dynamic load case (λ)	1.04	–
Wave resistance (R_w)	94.2	kN
Correlation allowance coefficient (C_A)	3.311×10^{-4}	–
Correlation resistance (R_A)	390	kN
Total resistance (R_T)	2740	kN

Table 5 – Output results of the power prediction model for LH2 tanker design.

Power prediction model parameters	Value	Units
The effective wake fraction (w)	0.213	–
Thrust dedication factor (t)	0.218	–
Relative rotational efficiency (η_R)	99.2	%
Effective horsepower for the ship hull (P_{EH})	25.4	MW
A speed of advance (V_A)	7.28	m/s
Propeller thrust required (T_H)	3503.5	KN
The ship required thrust horsepower (P_{TH})	26	MW
The hull efficiency (η_H)	100.6	%
The propulsive horsepower (P_{DH})	45.5	MW
Brake horsepower (P_{BH})	46	MW

Open-water propeller design and characteristics

The authors opted for a fixed-pitch twin-screw propeller arrangement for the JAMILA tanker. This selection was guided by the ship speed and power requirement considering the size of the JAMILA and in line with the maximum allowable unloaded draft. Additionally, the authors examined the three- and four-bladed propellers. A four-bladed propeller was

Table 6 – Propeller design parameters and performance.

Propeller characteristic	Value	Unit
Propeller type	Fixed pitch	–
Number of blades (Z)	4	–
Number of propellers	Twin-screw fixed on the pods	–
Propeller diameter (D_{pr})	6.4	m
Pitch ratio (P/D_{pr})	1.0	–
Blade area ratio (A_E/A_O)	0.9	–
Advance coffined (J)	0.54	–
Wake Fraction (w)	0.213	–
Thrust deduction (t)	0.218	–
Thickness to chord length ratio (t/c)	0.029	–
Propeller rotating speed (n)	124.8	RPM
Propeller clearances and material	**Value** (for each propeller)	**Unit**
Clearance between propeller tip and hull	1.66	M
Clearance between propeller tip and keel	0.2	M
Propeller material	Ni–Al Bronze (NAB/Nibral/Cu-3)	–
Propeller performance	**Value** (for each propeller)	**Unit**
Thrust Coefficient (K_T)	0.2528	–
Torque Coefficient (K_Q)	0.0418	–
Propeller thrust generated (T_{gh})	1852.6	KN
Propeller torque (Q)	311	KN.m
Open water efficiency (η_O)	56	%

selected because the efficiency was 56% greater than that of the three-blade propeller (54%).

The design of the propeller was based on the open-water characteristics of the Wageningen B-series propellers [16]. Consequently, the propeller thrust (K_T) and torque (K_Q) coefficients were expressed as polynomials in the J, P/D_{pr}, A_E/A_O, Z, R_n, and t/c by the following equations.

$$K_T = f_1(J,\ P/D_{pr}, A_E/A_O, Z, R_n, t/c) \tag{34}$$

$$K_Q = f_2(J,\ P/D_{pr}, A_E/A_O, Z, R_n, t/c) \tag{35}$$

where J is an advance ratio, P/D_{pr} denotes propeller pitch diameter ratio, A_E/A_O represents the propeller blade area ratio, Z is the blade number, R_n is the Reynold number, and t/c denotes the thickness to chord length ratio. The main propeller design parameters can be shown in Table 6.

The last stage of the propeller design was to investigate the non-cavitation criterion using the Aufer Keller equation.

$$A_E/A_O \geq K + \frac{(1.3+0.3Z)\cdot(T_h/2)}{D_{pr}{}^2(P_{atm}+\rho g h - P_v)}$$

$$A_E/A_O \geq 0.1 + \frac{(1.3+0.3\times 4)\cdot(1752)}{(6.4)^2(101.366+(1.025\times 9.81\times 3.4)-1.704)}$$

$$A_E/A_O \geq 0.89 \tag{36}$$

where h denotes the value of shaft immersion depth, Z represents the propeller blade number, g is the acceleration due to gravity, P_{atm} is the atmospheric pressure, P_v denotes the vapor pressure of water and the value of K = 0.1 for twin-screw ships. However, the value of $A_E/A_O = 0.9$, which is the mean value for the propeller satisfying the cavitation test [20].

Fig. 3 depicts the 3D design for the JAMILA fixed-pitch propeller that was designed using the Solid Work® design software. Explanatory, The black colour appears due to the choice of propeller blades material type, which is causes a surface reflection.

Azimuthal-podded propeller design

The propulsion system of JAMILA was designed as an efficient and applicable propulsion system owing to the large hull and small draft of the ship. The stern component of the LH2 carrier ship hull was designed with an unusual shape as compared with the conventional ships [3]. Consequently, this design allowed the authors to select the azimuthal thruster as a component of the LH2-carrier ship-propulsion system. This selection offered several solutions to achieve the optimum performance and logical design of the LH2-carrier ship-propulsion system in terms of accommodationist, manoeuvrability, reliability, and efficiency. In general, the azimuthal thruster propeller eradicated the shaft line, steering gear, rudder, and stern thrusters, which allowed to produce higher payloads at a greater speed for more effective operation with a smaller amount of energy from the power generators as compared with the usual axial propeller. Moreover, the azimuthal thruster exhibited brilliant manoeuvrability by offering full thrust in 360° operation, invisible noise and vibration, constant cruising speed, and substantial reduction of fuel consumption and GHG emission [24,25]. Specifically, in the case of the LH2 carrier ship, this selection caused the exclusion of the conventional inapplicable rudder from the designed LH2 ship owing to the shallow unloaded ship draft (9.263 m) [3]. The selection was based on the distance between the ship stern and keel, which was allowed limited accommodation of the designed dimensions for azimuthal pods, specifically for LH2 carrier ships. Moreover, the authors designed the system based on the Oasis-class cruise ship [26] in accordance with JAMILA power requirements. The JAMILA propulsion system comprised a turboelectric system including a combined-cycle gas turbine and azimuthal podded propeller of 50 M.W. The azimuthal-podded propeller pod propulsion design was inspired by XO2100, which was produced by ABB [27]. The design included two azimuthal-podded propellers with 15.5 MW maximum power output from each one. Fig. 4 illustrates the primary components of the JAMILA turboelectric propulsion system. Moreover, the turboelectric propulsion system of the LH2 carrier ship included a single-pressure combined-cycle gas turbine as the primary mover to produce the required mechanical power, four generators, ten switchboards, two propulsion transformers, ten frequency convertors, two propeller motors located inside the azimuthal thruster case house. The efficiency of the system components assumed optimal efficiency to achieve the propulsion power required and reducing the output power losses. Fig. 5 presents the 3D design for the azimuthal-podded propeller system and propeller. Additionally, The specifications of the electric propulsion system will be presented in Table 7.

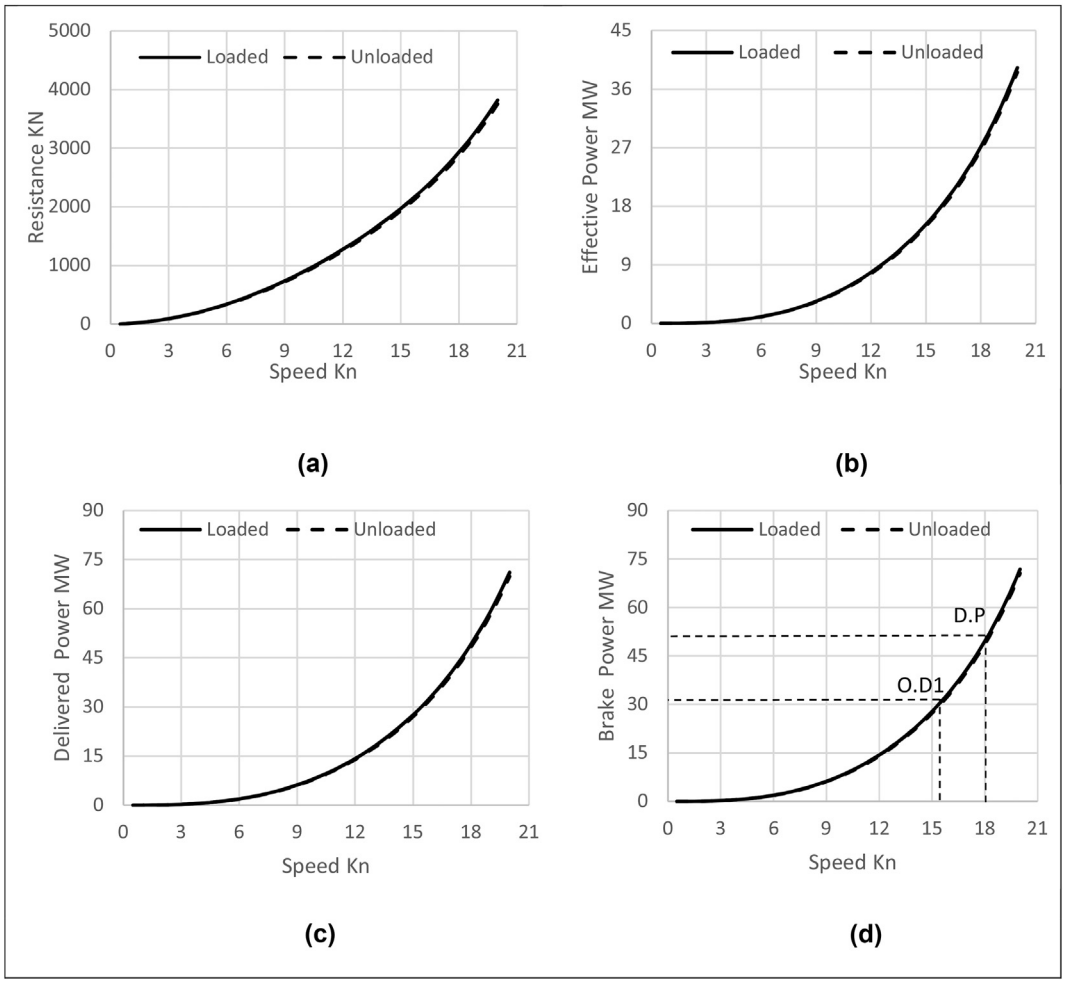

Fig. 2 – (a) Total resistance, (b) effective power, (c) delivered power, and (d) brake power estimated for the LH2 tanker for various speeds.

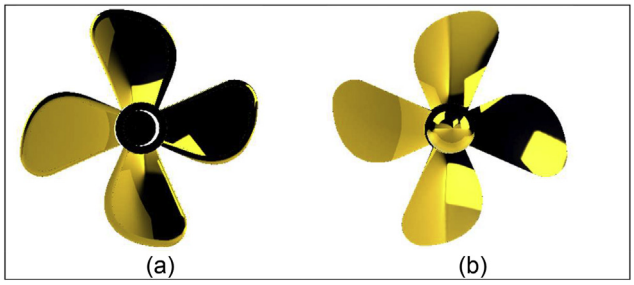

Fig. 3 – (a) Rear view of a four-blade propeller; (b) front view of a four-blade propeller.

COGAS powerplant

The authors decided to incorporate the combined-cycle gas turbine using hydrogen fuel in the design to achieve the twin objectives of high efficiency and carbon footprint elimination. As a result, the total installed power output was slightly larger than the power estimated in Power requirements. This condition provides a certain margin for conditions of high ambient temperature and gas turbine degradation. In addition, the gas turbine cycle was inspired by an existing advanced LM2500+ gas-turbine engine model that is frequently used for marine propulsion [28] and a single-pressure non-reheated steam cycle. The general specifications of the gas turbine and steam cycles are presented in Tables 8 and 9, respectively. Subsequently, both design and off-design analyses were conducted considering the variations in ambient temperature and component degradation, as shown in Fig. 6. The analyses were conducted using an in-house gas turbine performance software, TURBOMATCH using hydrogen as an alternative fuel and based on the gas turbine performance evaluation code [18] for conventional gas turbine performance [29].

Figs. 7 and 8 show the COGAS components with the single pressure HRSG and the heat recovery steam generator's heat transfer stages. However, the following model presents the combined-cycle performance calculation based on the following calculation steps [30,31].

The pinch-point temperature on the water side was calculated to determine the saturation relationship between pressure and temperature using the properties of fluid tables. The steam pressure value of 60 bar was obtained from the saturated water and steam table.

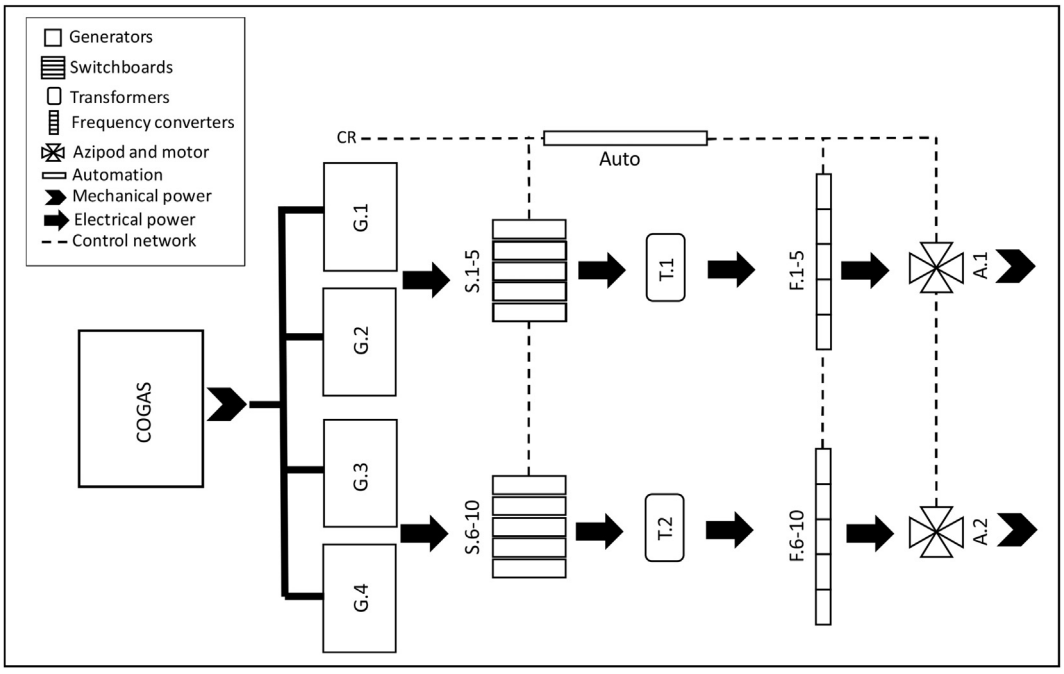

Fig. 4 – JAMILA Turbo-electric propulsion system components.

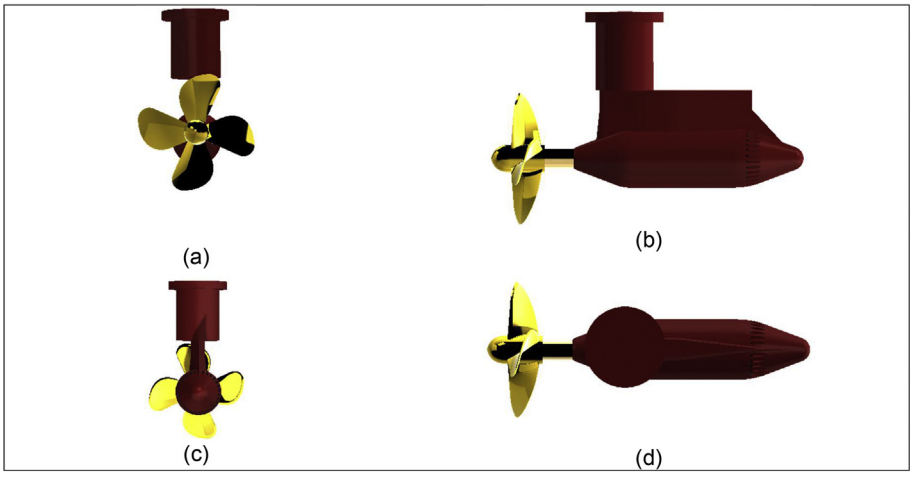

Fig. 5 – Turboelectric (a) front, (b) side, (c) rear, and (d) top views.

Table 7 – General specifications of electric propulsion system.

Azimuthal podded propeller general specifications	Value (for each azimuthal podded propeller)	unit
Number of units	2	–
Total horizontal azimuthal podded propeller length	11.5	m
Total weight	280	t
Output power	15.5	MW
Main motor supply voltage	3000	V

$$T_c = T_b \tag{37}$$

where T_c and T_b are the saturation temperatures. The pinch-point temperature on the gas side (T_3) can be calculated using the following equation.

$$T_3 = T_b + \Delta T_p, \tag{38}$$

where ΔT_p is the pinch-point temperature variation. The economiser outlet temperature (T_d) was simultaneously calculated using the following equation.

$$T_d = T_c - \Delta T_a \tag{39}$$

The heat exchanged in the above-mentioned pinch point was determined using the following equation.

Table 8 – General specifications of gas turbine cycle.

Gas Turbine Cycle	Values	Units
Ambient temperature	288.15	K
Ambient pressure	101.3	kPa
Pressure ratio	23.1	–
Specific fuel consumption	0.07416	kg/kw-h
Exhaust gas mass flowrate	84.948	kg/s
Exhaust gas temperature	840.3	K
Turbine inlet temperature	1550	K
Fuel flow	0.7485	kg/s
Power output	36.2	MW
Thermal Efficiency	40.3	%

Table 9 – General specifications of a steam cycle.

Steam plant parameters	values	units
superheat temperature (T_a)	559.8	C
Steam pressure (P_S)	60	Bar
Pinch point temperature difference (ΔT_p)	7.5	C
Approach point temperature difference (ΔT_a)	20	C
Steam mass flowrate (m_s)	10.51	kg/s
Condenser pressure (P_{cond})	0.06	Bar
Feed water temperature (T_e)	36.2	C
Steam turbine output power (W_{ST})	14.35	MW
Steam turbine isentropic efficiency (η_{ST})	89.9	%
Pump work (W_{pump})	4.1388	MW

$$Q_{1-3} = m_g.c_p.(T_1 - T_3) \tag{40}$$

where Q_{1-3} denotes the amount of heat captured by the water–steam circuit in the evaporator and superheater sections, so the following equation can be used with the water and steam enthalpy values to determine the steam mass flow. From the superheated steam table, 60 bar and 559.8 °C were selected for h_a, and from saturated water and steam table with respect to 60 bar for h_d [32].

$$m_s = \frac{Q_{1-3}}{h_a - h_d} \tag{41}$$

The following equation was used to calculate the amount of heat exchanged under the pinch point and is expressed by the water-side energy balance (evaluate h_e using the saturated water and steam table for 36.2 °C).

$$Q_{3-4} = Q_{e-d} = m_s \cdot c_p(T_d - T_e) \tag{42}$$

The following equation can be used to evaluate the Rankine cycle stack temperature.

$$Q_{3-4} = m_g \cdot c_p(T_3 - T_4) \tag{43}$$

The following equations were used to determine the steam turbine expansion. Moreover, the superheated steam temperature and pressure were required to find the steam turbine input enthalpy (h_i) and entropy (s_i), where $h_i = 3562.1 \frac{kJ}{kg}$ and $s_i = 7.05 \frac{kJ}{kg}$.

Furthermore, the condenser pressure (P_{cond}) is required to calculate the isentropic outlet steam quality (X) and the corresponding isentropic outlet steam enthalpy (h_{oiso}) and entropy (s_o), where $s_{og} = 8.329 \frac{kJ}{kgK}$, $s_{of} = 0.521 \frac{kJ}{kgK}$ and $h_{of} = 152 \frac{kJ}{kgK}$.

$$X = \frac{s_i - s_{of}}{s_{og} - s_{of}} \tag{44}$$

$$h_{oiso} = X \cdot h_{ofg} + (1 - X) \cdot h_{of} \tag{45}$$

$$h_{oact} = h_{oiso} + h_{of} \tag{46}$$

The isotropic efficiency (η_{ST}) of the steam turbine was determined as

$$\eta_{ST} = \frac{h_i - h_{oact}}{h_i - h_{oiso}} \tag{47}$$

The following equation was used to evaluate the steam turbine work (W_{ST}).

$$W_{ST} = m_s(h_i - h_o) \tag{48}$$

$$Wtotal_{ST} = W_{ST} - W_{pump} = 14.3 - 0.4 = 13.9\ MW \tag{49}$$

The Combined cycle total efficiency can be determined now by using the following equation.

$$W_{CC} = W_{GT} + W_{ST} \tag{50}$$

$$\eta_{CC} = \frac{\eta_{GT} \cdot (W_{GT} + W_{ST})}{W_{GT}} \tag{51}$$

Table 10 presented the output results of the COGAS model for liquefied hydrogen tanker design.

Fig. 9 portrays the COGAS powerplant output power and thermal efficiency in design and off-design conditions obtained using MATLAB software.

The results presented in Fig. 6a indicate that the output power of the gas turbine in design point was 36.2 MW at 15 °C and a TET of 1550 K. Additionally, the worst-case scenario of the gas-turbine output power was 20 M.W. at a turbine entry temperature of 1550 K and 6% degradation at 35 °C ambient temperature. Fig. 2d illustrates that the required ship brake power was 49 M.W. at 18 knots for the design point and 31 M.W. at 16 knots for the off-design point under completely loaded conditions. Moreover, Fig. 9a produce that the output power of the COGAS in the design point was 50 MW at 15 °C

Table 10 – Output results of COGAS model for LH2 tanker design.

COGAS model results	value	units
The saturation temperatures (T_c)	275.6	C
The pinch point temperature on the gas side (T_3)	283.1	C
Economiser outlet temperature (T_d)	255.6	C
Heat exchanged above the pinch (Q_{1-3})	24.7	MW
Steam mass flow (m_s)	10.51	kg/s
Heat transfer in gas side from HRSG (Q_{3-4})	2.7	MW
Rankine cycle stack temperature (T_4)	256	C
Outlet steam quality (X)	0.83	–
isentropic outlet steam enthalpy (h_{oiso})	2045	kj/kg
Actual outlet steam enthalpy (h_{oact})	2197	kj/kg
Steam turbine isotropic efficiency (η_{ST})	89.9	%
The steam turbine work (W_{ST})	14.36	MW
The total steam turbine work ($Wtotal_{ST}$)	13.9	MW
Combined cycle total output power (W_C)	50	MW
Combined cycle total efficiency (η_{CC})	55	%

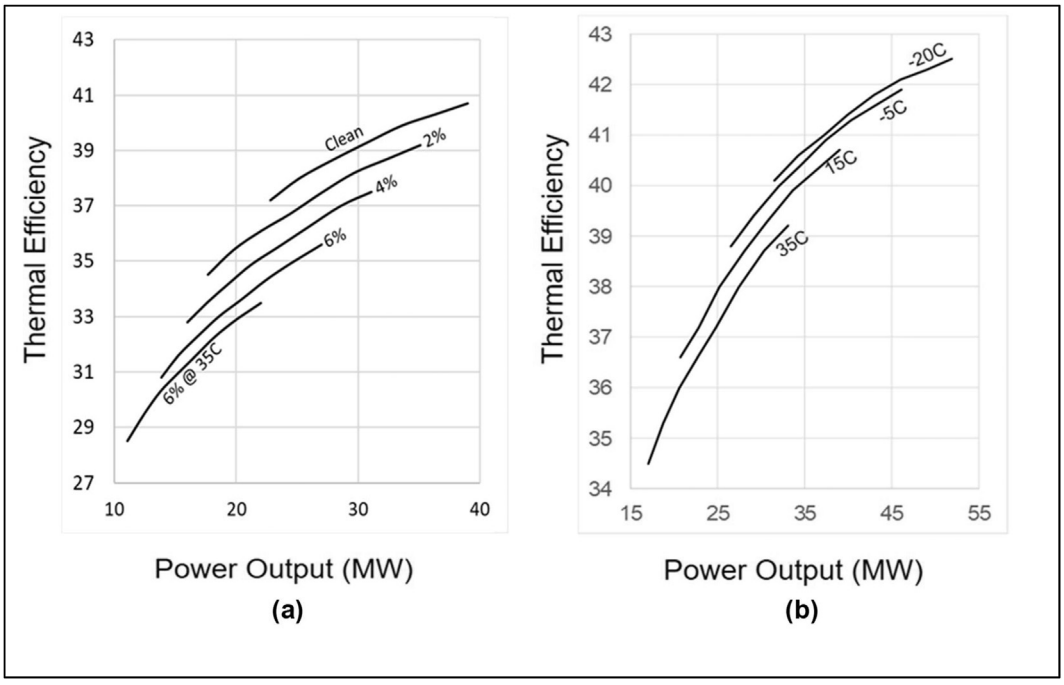

Fig. 6 – Gas turbine performance showing power output vs thermal efficiency (%). (a) Impact of degradation at a standard ambient temperature of 15 °C (Clean, 2%, 4%, and 6%) plus the influence of 6% degradation at an ambient temperature of 35 °C. (b) Gas turbine performance in clean conditions under the influence of ambient temperature.

and a TET of 1550 K that's offer 13.8 MW as an additional generated power compared with the simple cycle gas turbine. For validation and error estimation, around 0.5% was found as an error percentage between simulation results and formal calculations of the COGAS additional power generated. Fig. 9b depicts the total output power generated from COGAS was 50 M.W. at design point and 31 M.W. in the worst-case scenario. The slight deviation between the total power generated from the COGAS propulsion system and the power required for JAMILA allows a small margin for degradation and ambient temperatures. Thus, the proposed COGAS design appears as a suitable option to power JAMILA at its design speed of 18 knots and at 16 knots under adverse weather conditions in a degradation sailing scenario.

Overall, the thermal efficiency of 50–54% can be achieved under the most recurring operating circumstances, which is highly considered for a marine power plant. This efficiency was not as high as that of a land-based gas turbine operating with combined cycles at typically 57–61% because the cycle is intended for application in marine duty, and therefore, it must not be aggressive. Nonetheless, the efficiency of the designed marine power plant was adequately high for practical purposes. Moreover, several factors reduce the thermal efficiency of the marine combined-cycle gas turbine such as the small size of the gas-turbine components specifically for marine applications, sea-environmental effects, and the limitation of engine accommodation area onboard the ship [33,34]. However, a sizing exercise was not conducted in this study because the aft section of the ship was designed considering the characteristics of the Pulrose Power Station [35], which is familiar to one of the authors. Although this approach is not completely accurate, it provides confidence through a comfortable margin for the accommodation of the propulsion system.

Hydrogen propulsion system technical feasibility

Evaluation of the suggested unique propulsion system fuelled by hydrogen in this study based on technical feasibility is essential for achieving the maritime zero-emission target by 2025. The research results show several advantages of the propulsion system, making this propulsion system suitable for the future, specifically for hydrogen carrier ships. These benefits are centred through the combination of technical aspects such as the system design philosophy, engine high thermal efficiency, zero CO_2 emission, perfect controllability especially in shallow water and acceptable performance in design and off-design conditions compared with the current maritime propulsion systems. The following reasons show that the suggested propulsion system is feasible to apply in terms of the technical aspect.

- The results show that using a combined cycle gas turbine fuelled by hydrogen achieved 55% thermal efficiency with a zero CO_2 -emission advantage compared with 54.5% using conventional fuel.
- The simulation results show that the combined cycle gas turbine fuelled by hydrogen has an acceptable thermal efficiency and power output performance to be a successful propulsion system in 6% of degradation at different weather conditions.

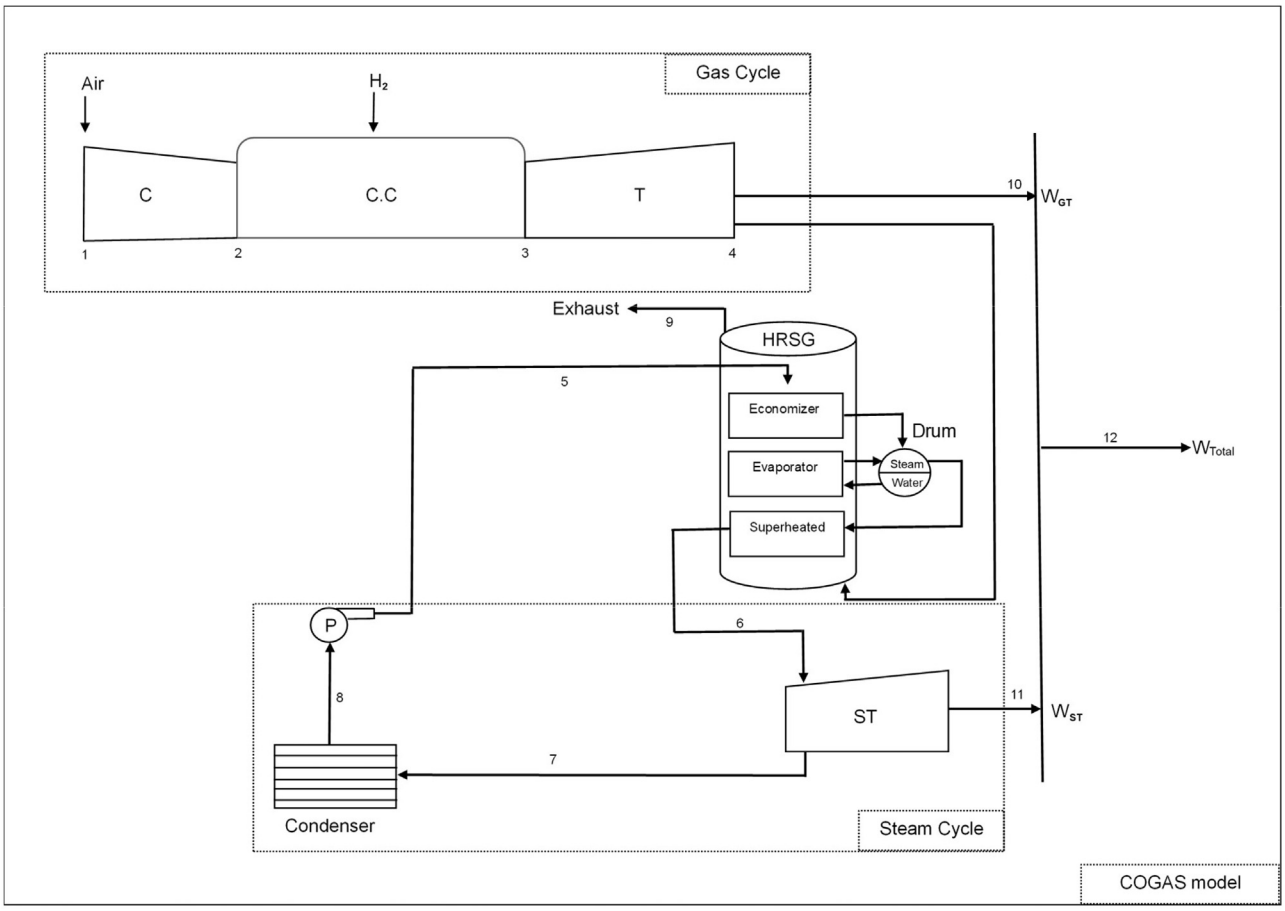

Fig. 7 – Combined cycle gas and steam turbine component. C: Compressor, CC: Combustor T: Turbine and S.T.: Steam Turbine.

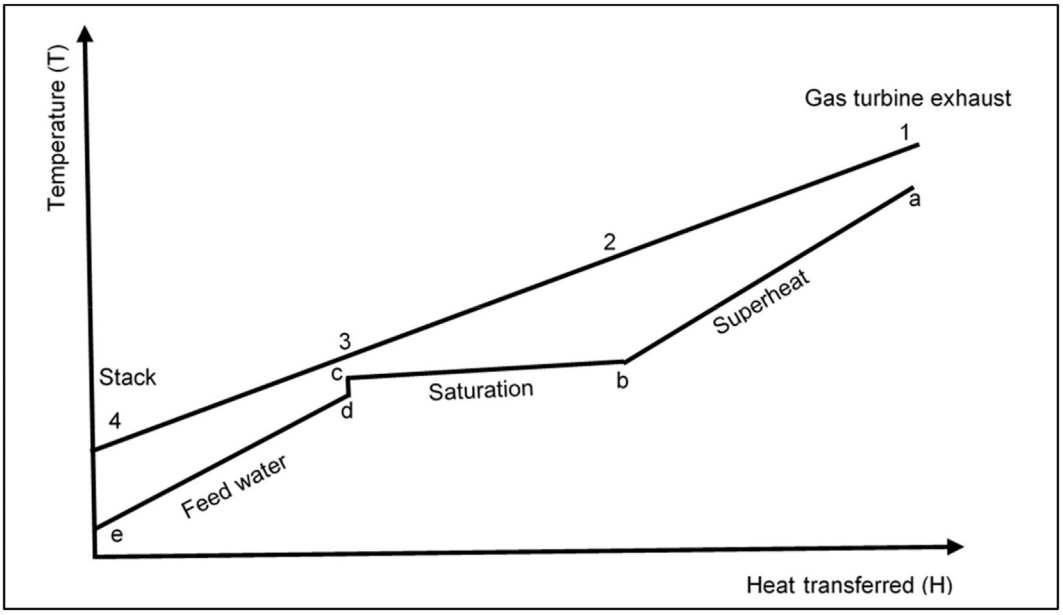

Fig. 8 – Heat transfer diagram for a single pressure HRSG.

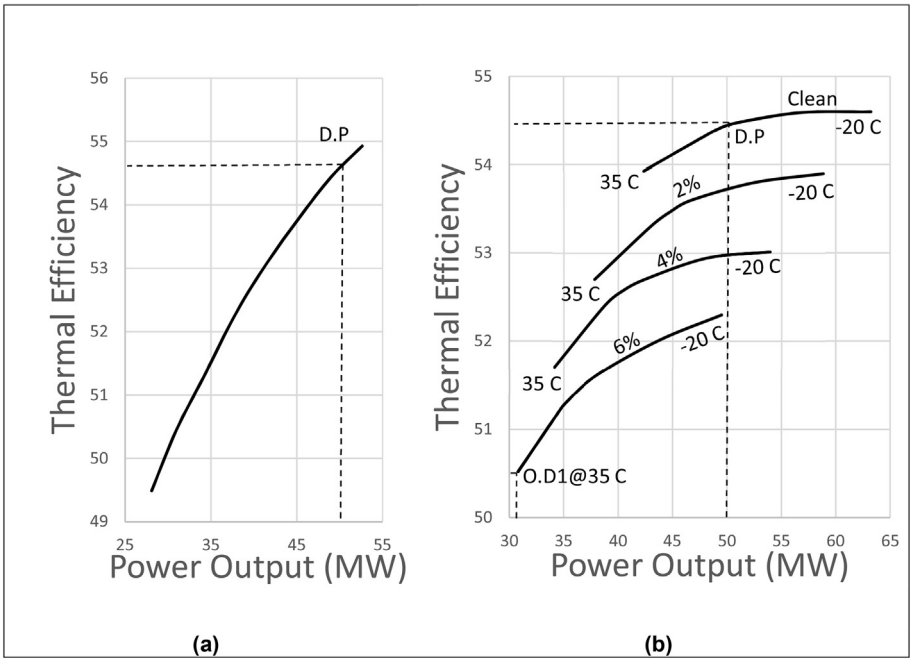

Fig. 9 – Performance depicting power output vs thermal efficiency (%). (a) COGAS performance according to Turbine Entry Temperature (TET) and clean conditions at an ambient temperature of 15 °C. (b) COGAS performance according to ambient temperature and degradation.

- The azimuthal thruster is the right choice causing exclusion of the conventional unapplicable rudder from the designed LH2 carrier ship due to the shallow unloaded ship draft (9.263 m). However, in the case of conventional maritime propulsion systems, the rudder is needed for the designed ship, which is an unlogic option due to the shallow ship draft, specifically in the liquefied hydrogen carrier ship.
- From an industrial point of view, the suggested maritime propulsion system fuelled by hydrogen is applicable and can be implemented with state-of-the-art techniques and tools [27,28].

Conclusions

This study determined the propulsion system characteristics of the JAMILA LH2 tanker. The power plant considered was a combined-cycle gas turbine, and the output design power was 50 M.W. The calculations suggested that ship requirement was 49 M.W. for 18 knots in case of completely loaded conditions in calm water. Subsequently, the simulation results suggested that this consideration was satisfied in majority of the operational cases even under conditions of degradation and increased ambient temperature. In the worst-case scenario of high degradation and ambient temperature, the proposed system still delivered 31 M.W. at a thermal efficiency greater than 50% allowing a ship speed of 16 knots.

Furthermore, the evaluation of the propulsion system identified the main features of the JAMILA, which was powered by a combined cycle to achieve an attractive thermal efficiency. Although a slightly more efficient power plant and propeller arrangement could be achieved with a detailed optimisation, the proposed system delivered a competitive performance and achieves the objective of presenting a visualisation of a potential LH2 tanker ship propulsion system.

Declaration of competing interest

The authors declare that they have no known competing financial interests or personal relationships that could have appeared to influence the work reported in this paper.

Acknowledgements

The authors are grateful toward the Government of the State of Kuwait and the Public Authority for Applied Education and Training (PAAET) for the provisions and the financial support.

REFERENCES

[1] IMO. Report of the marine environment protection committee on its 72nd session. 2018. MEPC 72/WP.7.
[2] U.K. Department of Transport. Clean maritime plan. London: U.K. DoT; 2019.
[3] Alkhaledi ANFNR, Sampath S, Pilidis P. A hydrogen fuelled LH2 tanker ship design. Ships Offshore Struct 2021. https://doi.org/10.1080/17445302.2021.1935626.
[4] Bourne S. The future of fuel: the future of hydrogen. Fuel Cell Bull 2012;1:12–5. https://doi.org/10.1016/S1464-2859(12)70027-5.

[5] Sharma S, Ghoshal SK. Hydrogen the future transportation fuel: from production to applications. Renew Sustain Energy Rev 2015;43:1151–8. https://doi.org/10.1016/j.rser.2014.11.093.

[6] Bazzanella AM, Ausfelder F. Low carbon energy and feedstock for the European chemical industry. DECHEMA Gesellschaft für Chemische Technik und Biotechnologie; 2017 (In German).

[7] Armellini A, Daniotti S, Pinamonti P, Reini M. Evaluation of gas turbines as alternative energy production systems for a large cruise ship to meet new maritime regulations. Appl Energy 2018;211:306–17.

[8] Haglind F. A review on the use of gas and steam turbine combined cycles as prime movers for large ships. Part II: previous work and implications. Energy Convers Manag 2008;49:3468–75.

[9] Sannemann BN. Pioneering gas turbine-electric system in cruise ships: a performance update. Mar Technol SNAME News 2004;41(4):161–6.

[10] Benvenuto G, Campora U, Laviola M. Assessment of steam cycle layouts for COGAS ship propulsion systems. In: Proceedings of the 2nd international conference on maritime technology and engineering (MARTECH 2014); 2014. p. 15–7. https://doi.org/10.1201/b17494-99. Lisbon.

[11] Benvenuto GY, Bertetta DT, Carollo FM. COGAS plant as possible future alternative to the diesel engine for the propulsion of large ships. In: Sustainable maritime transportation and exploitation of sea resources; 2011. 978-0-415-62081-9.

[12] Doulgeris G, Korakianitis T, Pilidis P, Tsoudis E. Techno-economic and environmental risk analysis for advanced marine propulsion systems. Appl Energy 2012;99:1–12.

[13] Talluri L, Nalianda DK, Kyprianidis KG, Nikolaidis T, Pilidis P. Techno-economic and environmental assessment of wind assisted marine propulsion systems. Ocean Eng 2016;121:301–11. https://doi.org/10.1016/j.oceaneng.2016.05.047.

[14] Holtrop J, Mennen GGJ. An approximate power prediction method. Int Shipbuild Prog 1982;29:166–70.

[15] Holtrop J. A statistical re-analysis of resistance and propulsion data. Int Shipbuild Prog 1984;31:272–6.

[16] Oosterveld M, van Oossanen P. Further computer analysed data of the Wageningen B-screw series. Int Shipbuild Prog 1975;22:251–62.

[17] Dzida M, Olszewski W. Comparing combined gas turbine/steam turbine and marine low speed piston engine/steam turbine systems in naval applications. Pol Marit Res 2011:43–8.

[18] Nikolaidis T. TURBOMATCH– gas turbine performance simulation –user manual. unpublished: Cranfield University; 2017.

[19] Enable H_2 Website. 2020. https://www.enableh2.eu/. [Accessed 11 April 2020].

[20] Roh MI, Lee KY. Computational ship design. Singapore: Springer; 2018.

[21] ITTC. Fresh water and seawater properties. ITTC Procedure 2011;7. 5-02-01-03.

[23] Lamb T. Ship design and construction vol. ii. SNAME; 2003. ISBN No. 0-939773-41-4.

[24] Kobyliński L. Transport. Problems of handling ships equipped with AZIPOD propulsion systems. Prace Naukowe Politechniki Warszawskiej 2013;95:231–45.

[25] Wang H. Report on the development of cruise industry in China2019. Singapore: Springer; 2018.

[26] Ye X, Wang X, Wang Y, Luo Y, Yang G, Sun R. Design features and construction enlightenments of oasis-class luxury cruise ships. In: Report on the development of cruise industry in China. 2019. Singapore: Springer; 2018. p. 201–18.

[27] ABB. Azipod® XO2100 and XO2300 product introduction. https://searchext.abb.com/library/Download.aspx?DocumentID=3AFV6016618&LanguageCode=en&DocumentPartId=&Action=Launch. [Accessed 17 August 2020].

[28] Luck DL. Extending use of marine gas turbines through application of the LM2500+. In: Proceedings of the ASME 1998 international gas turbine and aeroengine congress and exhibition. vol. 2. Aircraft Engine; Marine; Microturbines and Small Turbomachinery. ASME; 1998. https://doi.org/10.1115/98-GT-0411998. V002T03A001.

[29] Palmer JR, Pilidis P. Gas turbine theory and performance, thermal power MSc course notes. Cranfield University; 2013. unpublished.

[30] Cengel YA, Boles MA. Thermodynamics: an engineering approach. McGraw-Hill Education; 2014.

[22] ITTC. S.F. turbulence committee report. In: Proc. 8th international towing tank conference; 1957. p. 71–227.

[31] Jefferson M, Zhou PL, Hindmarch G. Analysis by computer simulation of a combined gas turbine and steam turbine (COGAS) system for marine propulsion. J Mar Eng Technol 2003;2:43–53. https://doi.org/10.1080/20464177.2003.11020164.

[32] Cengel YA, Boles MA, Kanoglu M. Thermodynamics: an engineering approach. New York: McGraw-hill; 2011.

[33] Altosole M, Benvenuto G, Campora U, Laviola M, Trucco A. Waste heat recovery from marine gas turbines and diesel engines. Energies 2017;10(5):718.

[34] Haglind F. A review on the use of gas and steam turbine combined cycles as prime movers for large ships. Part II: previous work and implications. Energy Convers Manag 2008;49(12):3468–75.

[35] Manx Utilities. https://www.manxutilities.im/about-us/our-assets/electricity/power-stations/. [Accessed 20 December 2020].

[36] Evrin RA, Dincer I. Thermodynamic analysis and assessment of an integrated hydrogen fuel cell system for ships. Int J Hydrogen Energy 2019 Mar 8;44(13):6919–28.

[37] Li F, Yuan Y, Yan X, Malekian R, Li Z. A study on a numerical simulation of the leakage and diffusion of hydrogen in a fuel cell ship. Renew Sustain Energy Rev 2018 Dec 1;97:177–85.

[38] Mao X, Ying R, Yuan Y, Li F, Shen B. Simulation and analysis of hydrogen leakage and explosion behaviors in various compartments on a hydrogen fuel cell ship. Int J Hydrogen Energy 2021 Feb 3;46(9):6857–72.

[39] McKinlay CJ, Turnock SR, Hudson DA. Fuel cells for shipping: to meet on-board auxiliary demand and reduce emissions. Energy Rep 2021 May 1;7:63–70.

[40] McKinlay CJ, Turnock SR, Hudson DA. Route to zero emission shipping: hydrogen, ammonia or methanol? Int J Hydrogen Energy 2021 Aug 10;46(55):28282–97.

[41] Palmer JR, Pilidis P. Gas turbine theory and performance, thermal power MSc course notes. unpublished: Cranfield University; 2013.

[42] Haglind Fredrik, Singh Riti. Design of aero gas turbines using hydrogen. 2006. p. 754–64.

2022-05-11

Propulsion of a hydrogen-fuelled LH2 tanker ship

Alkhaledi, Abdullah N. F. N. R.

Elsevier

Alkhaledi ANFNR, Sampath S, Pilidis P. (2022) Propulsion of a hydrogen-fuelled LH2 tanker ship, International Journal of Hydrogen Energy, Volume 47, Issue 39, May 2022, pp. 17407-17422
https://doi.org/10.1016/j.ijhydene.2022.03.224